

## PREDICTION OF NANOFLUID THERMAL CONDUCTIVITY AND VISCOSITY WITH MACHINE LEARNING AND MOLECULAR DYNAMICS

by

**Freddy AJILA<sup>a\*</sup>, Saravanan MANOKARAN<sup>b</sup>, Kanimozhi RAMASWAMY<sup>b</sup>,  
Devi THIYAGARAJAN<sup>c</sup>, Praveen PAPPULA<sup>d</sup>, Mohammed ALI SHAIK<sup>d</sup>,  
Surrya Prakash DILLIBABU<sup>e</sup>, Uday Kiran KASI<sup>f</sup>, and Mayakannan SELVARAJU<sup>g</sup>**

<sup>a</sup> Facultad de Informática y Electrónica, Escuela Superior Politécnica de Chimborazo (ESPOCH),  
Sede Orellana, El Coca, Ecuador

<sup>b</sup> Department of Electronics and Communication Engineering, Faculty of Engineering and Technology,  
Annamalai University, Annamalai Nagar, Chidambaram, Tamilnadu, India

<sup>c</sup> Department of Computer Science and Engineering, Saveetha School of Engineering,  
Saveetha Institute of Medical and Technical Sciences, Saveetha University, Chennai, India

<sup>d</sup> School of Computer Science and Artificial Intelligence, SR University,  
Warangal, Telangana State, India

<sup>e</sup> Department of Mechanical Engineering,  
Vel Tech Rangarajan Dr. Sagunthala R&D Institute of Science and Technology,  
Chennai, Tamil Nadu, India

<sup>f</sup> Department of Electronics and Communication Engineering,  
Guntur, Vijayawada, Andhra Pradesh, India

<sup>g</sup> Department of Mechanical Engineering, Vidyaa Vikas College of Engineering and Technology,  
Tiruchengode, Namakkal, Tamilnadu, India

Original scientific paper  
<https://doi.org/10.2298/TSCI230312005A>

*It is well-known that nanofluids differ significantly from traditional heat transfer fluids in terms of their thermal and transfer characteristics. Two of CO<sub>2</sub> transfer characteristics, its thermal conductivity and its viscosity, are crucial to improved oil retrieval methods and industries refrigeration. By combining molecular modeling with various machine learning algorithms, this study predicts the conduction characteristics of iron oxide CO<sub>2</sub> nanofluids. It is possible to evaluate the accuracy of these transfer parameter estimates by applying machine learning methods such as decision tree, K-nearest neighbors, and linear regression. Predicting these transfer qualities requires knowing the size, fraction of nanoparticle volume, and temperature. To determine the characteristics, molecular dynamics simulations are run using the large-scale atom Vastly equivalent simulant. An inter- and intra-variable Pearson correlation was established to confirm that the input variables were reliant on  $m$  and thermal conductivity. The results were finally confirmed by using statistical coefficients of determination. For a variety of temperature ranges, volume fractions, and nanoparticle sizes, the study found that the decision tree model was the best at predicting the transport parameters of nanofluids. It has a 99% success rate.*

**Key words:** thermal conductivity, viscosity, machine learning, nanofluids,  
volume fraction

\* Corresponding authors, e-mail: [freddy.ajila@epoch.edu.ec](mailto:freddy.ajila@epoch.edu.ec)

## Introduction

Dispersed solid nanoparticles or nanofibers, usually measuring 1-200 nm, characterise new classes of fluids called *nanofluids*. [1]. There have been significant advancements in the transfer properties of nanofluids, such as thermal conductivity,  $k$ , compared to conventional heat transfer fluids [2]. Improving CO<sub>2</sub> thermophysical characteristics for use as a refrigerant and oil recovery agent is the primary goal of this investigation. Using its nanofluid in conjunction with iron oxide nanoparticles, np, is one example. A study conducted by the authors found that the thermal efficiency of a solar collector could be enhanced by 16% and 21%, respectively, by adding nanoparticles of CuO and Fe<sub>2</sub>O<sub>3</sub> to water [3]. Water treated with nanostructures of multi-walled carbon nanotubes improved the performance of PV/thermal systems, according to another study. Research using nanofluid in parabolic trough collectors found that increasing the thermal efficiency of the system by 0.76% was possible by adding CuO nanoparticles to the utilised motor oil [4]. Even in contexts unrelated to renewable energy, nanofluids show promise for a variety of uses. The authors state that nanofluids can decrease the temperature of solar systems and make heat pipes and exchangers more efficient [5]. Nanofluids outperform pure fluids in terms of efficiency enhancement in thermal devices [6]. Their investigation into the effects of ferrofluid on heat pipes revealed that, in comparison pure water, which reduced thermal resistance very little, ferrofluid reduced thermal resistance by up to 75.8%. A large body of literature supports the idea that nanofluids can improve heat transmission [7].

Thermophysical properties like as viscosity,  $\mu$ , should also be determined. Since nanofluid is a combination of solids and liquids, its molecular weight is expected to be greater than that of a typical fluid. Recent studies have indicated that intrinsic features of nanofluids, like temperature, and size, percentage volume of particle,  $\phi$ , and particle shape impact on  $m$ , even though the majority of research indicates that dispersing nanoparticles improves  $m$ . Researchers looked into the Fe<sub>2</sub>O<sub>3</sub>-water  $\mu$  and discovered that it gets better as the temperature of the system and the concentration of Fe<sub>2</sub>O<sub>3</sub> rise. An increase of 86% in  $m$  was demonstrated by Wang *et al.* [8] for an  $n$ -Fe<sub>2</sub>O<sub>3</sub> size of 28 nm. As the diameter of the  $n$ -Fe<sub>2</sub>O<sub>3</sub> increased, Said *et al.* [9] demonstrated that  $\mu$  improved. As the np size increases, they found that  $\mu$  for Fe<sub>2</sub>O<sub>3</sub> nanofluids decreases. As Zhang *et al.* [10] points out, it is challenging to regulate the shape and size of np during experiments, thus simulations are used to evaluate the transfer properties under certain assumptions. Additional insights can be gleaned from these simulations by acquiring a more comprehensive and useful view of molecule structure properties.

Presently, efforts are being made to enhance CO<sub>2</sub>'s transfer properties, making it a more effective refrigerant and helping to improve oil recovery. Using molecular dynamics simulations, we have calculated the impact of particle size,  $\phi$ , and temperature on the Fe<sub>2</sub>O<sub>3</sub>-CO<sub>2</sub> nanofluid using LAMMPS, an open-source-code large-scale atomic/molecular massively parallel simulator [11]. From 350-700 K, there is a variance in nanoparticle size,  $\phi$ , and temperature ranging from 0.9% to 2.9%. Afterwards, the  $k$  and  $\nu$  of the Fe<sub>2</sub>O<sub>3</sub>-CO<sub>2</sub> nanofluid are modelled using machine learning (ML) techniques. This is done by determining the relevance of the input variables to  $k$  and  $\nu$  and then building a correlation between the dependent and independent variables. In order to anticipate the parameters of the transport of Fe<sub>2</sub>O<sub>3</sub>-CO<sub>2</sub> nanofluids, the outcomes of the molecular dynamics (MD) simulations were compared using several ML algorithms. As the np diameter grows, a denser area surrounding the np were seen also called the nanolayer, which may be contributing to the improved transport characteristics of the nanofluid as it is right now. In this study, the Pearson correlation were used that is obtained by ML to find the  $k$  and  $\mu$  of the Fe<sub>2</sub>O<sub>3</sub>-CO<sub>2</sub> nanofluid for varied input values with fewer simulations.

## Methodology and simulation system

As a method for simulating fluid-solid interactions and for testing the systems' thermal and transfer characteristics, MD simulations have been increasingly used in recent years [12]. In order to find the atomic interaction potential, an appropriate potential energy function was used to assess the interatomic forces.

Every contact is a part of the potential energy function. The potential's stored energy is located in bond-flexibility and angle bending, whereas non-bonded attraction and repulsion are mediated by Van der Waals forces. One way to assess the Coulombic interactions is by the use of the PPPM method [13]. Here, LAMMPS was used to simulate an Fe<sub>2</sub>O<sub>3</sub> np suspension in gaseous and supercritical CO<sub>2</sub>. In previous research, the characteristics of bulk CO<sub>2</sub> was identified using the TraPPE flexible CO<sub>2</sub> model. Lennard-Jones 12-6 potential, eqs. (1)-(3), and long-range electrostatic (Coulombic) potential,  $U$ , are examples of interatomic interactions [14]:

$$U_{ij}^{nb} = U_{ij}^{LJ} + U_{ij}^{Coulombic} \quad (1)$$

$$U_{ij}(r_{ij}) = 4\varepsilon_{ij} \left[ \left( \frac{\sigma_{ij}}{r_{ij}} \right)^{12} - \left( \frac{\sigma_{ij}}{r_{ij}} \right)^6 \right] \quad (2)$$

$$U_{ij}^{LJ}(r_{ij}) = \begin{cases} U_{ij}(r_{ij}) - U_{ij}(r_c) & r_{ij} < r_c \\ 0 & r_{ij} > r_c \end{cases} \quad (3)$$

where  $r_{ij}$  is the interatomic distance,  $\sigma_{ij}$  and  $\varepsilon_{ij}$  – the Lennard Jones parameters, and  $r_c$  – the cutoff radius.

Since the thermophysical properties are considered to be virtually independent thereafter, the cutoff radius is set to  $4\sigma_{o-o}$ .

To find the interatomic forces between various atomic types, one employs the Lorentz-Berthelot (LB) rule, which is based on [15]:

$$\sigma_{ij} = \frac{\sigma_{ii} + \sigma_{jj}}{2} \quad (4)$$

$$\varepsilon_{ij} = \sqrt{\varepsilon_{ii}\varepsilon_{jj}} \quad (5)$$

The forces between molecules of Fe<sub>2</sub>O<sub>3</sub> and CO<sub>2</sub> can be estimated using the LB rule, as demonstrated in our previous work [16].

In terms of electrostatic attraction and repulsion:

$$U_{ij}^{Coulombic} = \frac{1}{4\pi\varepsilon_0} \frac{q_i q_j}{r_{ij}} \quad (6)$$

where  $\varepsilon_0$  is the dielectric constant for vacuum and  $q_i$  and  $q_j$  – the charges on variant atoms.

To include the bond stretching and angle bending in the completely flexible CO<sub>2</sub> model, an extra potential function is utilised:

$$U_M(r_{ij}) = k_{Morse} \left[ 1 - e^{-\gamma(r_{ij}-r_0)} \right]^2 \quad (7)$$

$$U_H(\theta_{ijk}) = \frac{1}{2} k_{Harmonic} \left[ \theta_{ijk} - \theta_0 \right]^2 \quad (8)$$

where the bond and angular stretching are described by  $U_M$  and  $U_H$ , respectively, using Morse and Harmonic potentials with force constants  $k_{Morse}$  and  $k_{Harmonic}$ , respectively. The interatomic

distance is denoted by  $r_{ij}$ , while the equilibrium bond distance is represented by  $r_0$ . Similarly, the equilibrium angle between atoms is represented by  $\theta_0$ , and  $\theta_{ijk}$  is the angle between atoms. The CO<sub>2</sub> and other potential constants can be found in tab. 1, which also contains the necessary details for LAMMPS modelling.

**Table 1. Parameters determined by Lennard Jones for the TraPPE flexible CO<sub>2</sub> model using the force constants and atomic interactions between C and O**

Model	$\sigma_{O-O}$ [Å]	$\sigma_{C-C}$ [Å]	$\epsilon_{C-C}$ [K]	$\epsilon_{O-O}$ [K]
TraPPE <sub>flexible</sub>	3.07	2.84	28.3	80.4

where  $\gamma = 2.45$  and  $k_{\text{harmonic}} = 1.246$  kJ/mol rad<sup>2</sup>,  $k_{\text{Morse}} = 2.023$  kJ/mol Å<sup>2</sup>.

The atomic interactions of Fe<sub>2</sub>O<sub>3</sub> are described using potential interaction functions, charge-induced dipoles, steric-size effects, electrostatic and van der Waals contacts, and two- and three-body possibilities. At the outset, MD simulations are conducted using a conventional ensemble  $NVT$ , where  $T$ ,  $N$ , and  $V$  are constants representing the volume of the simulation box; VMD is then used for configuration visualization [17]. A 1 femtosecond time-step for the simulation was used to run the post-processing because it was found that this was sufficient for energy conservation. To ensure the accuracy of the simulation, the gaseous and supercritical CO<sub>2</sub> base fluids' thermophysical characteristics were computed between 350-750 K, maintaining a constant density of 150 kg/m<sup>3</sup>. Green-Kubo provides the formalism for estimating these transport parameters, and our experimental results have been validated with error rates of 0.52% for  $k$  and 0.76% for  $\nu$ . We have completed ten independent runs in order to get the mean values of thermal conductivity,  $k$ , and viscosity,  $\mu$ . The Nose-Hoover thermostat [18] was used to maintain a consistent temperature during the simulations.

A 3-D simulation domain was constructed for the bulk nanofluid by applying periodic boundary conditions to the base fluid and np. In both the gaseous and supercritical phases, the base fluid density remains at 150 kg/m<sup>3</sup> when the pressure is changed up to 250 bar within the temperature limits of 350-750 K. For each simulation domain, the volume percent was adjusted between 0.9% and 2.6%. The next step is to minimize in order to remove the near interactions that cause collisions with high potential energy and spread them apart. Maintaining a constant np allowed for sufficient time steps to bring each CO<sub>2</sub> molecule to its own equilibrium state. The Langevin thermostat and the  $NVE$  microcanonical ensemble are used for this purpose. By maintaining molecular immobility, the equilibrium state of np was reached by repeating the same technique. After reaching equilibrium, the entire simulation domain is run through the canonical ensemble test to find out the nanofluid's thermophysical characteristics. For each nanofluid system in the  $NVE$  ensemble, the Green-Kubo relations evaluate  $k$  and  $m$  by analysing the variation of autocorrelations. A numerical method for determining the locations and particle velocity in MD, the velocity Verlet algorithm, can track the changing atomic positions and velocities throughout the simulation by incorporating Newton's equation of motion. Loup Verlet developed this algorithm in the 1960's. The Green-Kubo formalism in molecular dynamics equilibrium finds the  $k$  at times 0 and  $t$  using the heat flow autocorrelation function [19]:

$$k = \frac{V}{3k_B T^2} \int \langle J(0) \cdot J(t) \rangle dt \quad (9)$$

$$\text{Heat flux vector } J = \frac{1}{V} \left[ \left[ \sum_{j=1}^N e_j v_j - \sum_{\alpha=1}^2 h_\alpha \sum_{j=1}^{N_\alpha} v_{\alpha j} \right] + \frac{1}{2} \left[ \sum_{i=1}^N \sum_{j=1, j \neq i}^N r_{ij} (v_j F_{ij}) \right] \right] \quad (10)$$

where  $F_{ij}$  is the attractive force between two atoms as a result of their paired interaction:

$$\text{Surplus energy}(e_j) = \sum_j \frac{1}{2} m_j v_j^2 + \sum_j \frac{1}{2} U_{ij} \quad (11)$$

where  $v_j$  is the velocity for the atom  $j$ :

$$\text{Mean partial enthalpy}(h_\alpha) = \frac{1}{N_\alpha} \sum_{j=1}^{N_\alpha} (e_j + e_j F_j) \quad (12)$$

The  $h_\alpha$  component is significant for calculating the  $k$  of a nanofluid system. Since average velocity does not exist for a system made up completely of fluid,  $h_a = 0$ . On average, nanofluids have a non-zero partial enthalpy. By shifting our attention from the mean partial enthalpy in the conventional Green-Kubo method to the energy flux for the conduction, we were able to accurately determine the nanofluid's  $k$  value. Equation (13) of the Green-Kubo formalism for equilibrium molecular dynamics computes the  $\mu$  by integrating the autocorrelation function:

$$\mu = \frac{V}{k_B T} \int_0^\infty P_{\alpha\beta}(0) P_{\alpha\beta}(t) dt, \quad \alpha, \beta = x, y, z \quad (13)$$

$$\text{Pressure tensor } P_{\alpha\beta}^{xy} = \sum_{k=\alpha}^{\beta} \sum_{i=1}^{N_\alpha} m_i^\alpha v_{xi}^\alpha v_{yi}^\beta + \sum_{k=\alpha}^{\beta} \sum_{i=\alpha}^{\beta} \sum_{i=1}^{N_k} \sum_{j \geq i}^{N_l} \left[ r_{ij}^{kl} e_x \left( \frac{\partial U(r_{ij}^{kl})}{\partial r_{ij}^{kl}} e_y \right) \right] \quad (14)$$

where  $r_{ij}^{kl}$  is the distance among two variant atoms  $i$  and  $j$  of type  $k$  and  $l$ ,  $m_i^\alpha$  – the mass,  $N_k$  – the number of atoms of  $k$  type,  $v_{xi}^\alpha$  – the velocity, and  $U(r_{ij}^{kl})$  – the energy interaction among the atoms.

All planes, *i.e.*,  $P_{xy}$ ,  $P_{xz}$ , and  $P_{yz}$ , are viewed as autocorrelation functions in order to carry out the  $\mu$  computation of the nanofluid.

Table 2 shows the first set-up, which was created by making similar combinations for varying volume percentages while keeping the CO<sub>2</sub> density constant. Visualization and radial distribution function analysis were used in our earlier work to verify that CO<sub>2</sub> existed in both gaseous and supercritical phases. In fig. 1(a), the experimental data and the estimated thermo-physical characteristics of the base fluid (gaseous CO<sub>2</sub> and supercritical CO<sub>2</sub>) are shown against each other.

**Table 2. Using a constant  $\rho = 150 \text{ kg/m}^3$  of the base fluid, the nanofluid compositions of Al<sub>2</sub>O<sub>3</sub>-CO<sub>2</sub>,  $\phi = 0.9\%$  are summarised; the same logic applied to the other volume fractions as well**

Nanoparticles diameter [nm]	Number of CO <sub>2</sub> atoms	Box dimensions [Å]	Number of iron oxide atoms
1.5	376	38	70
2.5	2998	79	520
3.5	9628	117	1760
4.5	22834	156	3990
5.5	44674	195	7750
6.5	77320	234	13330

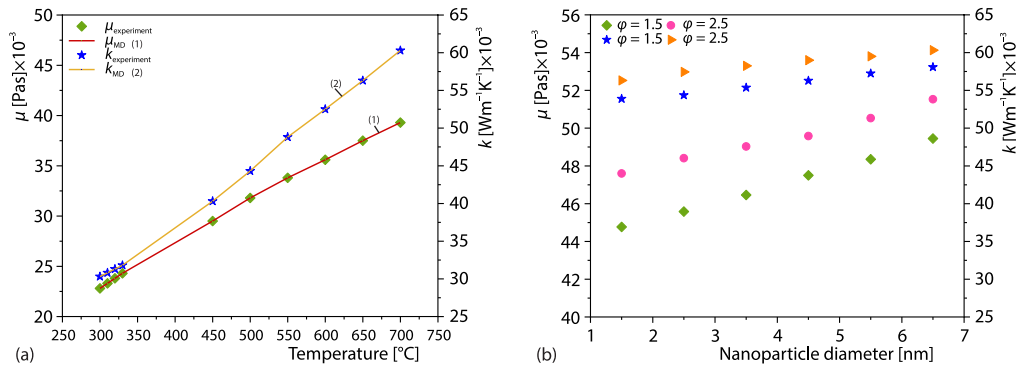


Figure 1. The experimental data were used to compare the  $k$  and  $\mu$  of; (a) bulk CO<sub>2</sub> and (b) nanofluids with 1.5 and 2.5 nm diameters to  $\phi$  at 550 K in the supercritical phase

## Results and discussions

### Impact of temperature on $k$ and $i$

The gas and supercritical Fe<sub>2</sub>O<sub>3</sub>-CO<sub>2</sub> nanofluids were used with varied volume fractions and temperatures ranging from 350 K to 700 K in this section see how temperature affected  $k$  and  $\mu$ . Figure 2 displays the computed MD findings, which demonstrate that the ther-

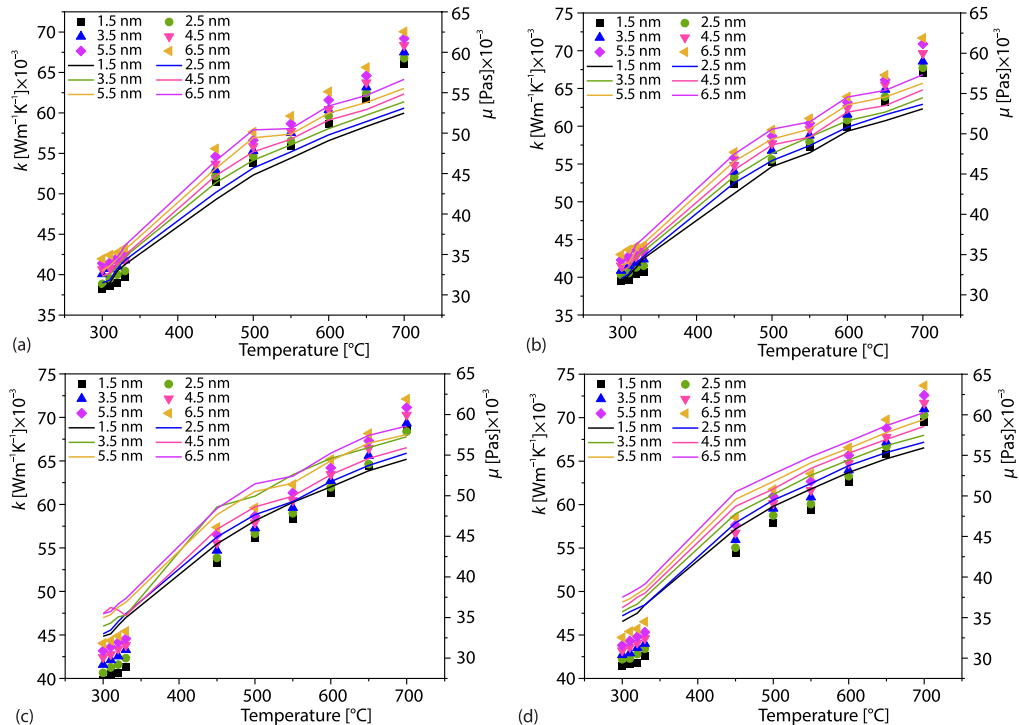


Figure 2. Observing the temperature effect involves altering nanoparticles diameters in the gas and supercritical stage, which cause variations in  $k$  and  $\mu$  at different percentage volume between 0.9% and 2.6%

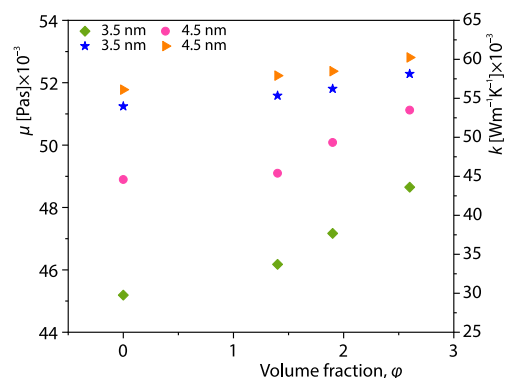
mophysical properties grow in relation temperature, with a stronger impact at greater  $\phi$ . The molecules were seen to be migrating rapidly toward the solid-fluid boundary and experiencing intense adherence by the nanoparticles as the temperature increased. At higher temperatures, the enhanced performance is due to the creation of a structural layer surrounding a bigger nanoparticles. The results of this work are consistent with those of previous research on various nanofluids. The findings of these research demonstrate that the characteristics increase in direct proportion the system's temperature.

**Volume fraction of nanoparticles and particle size impact on thermal conductivity and viscosity**

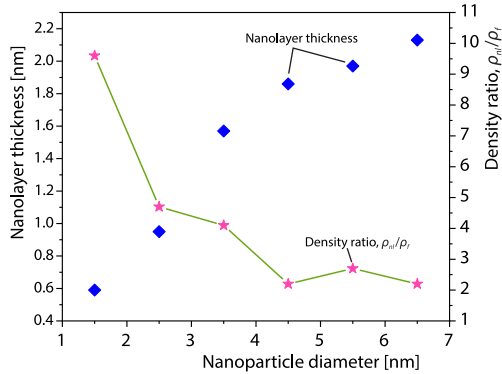
The influence of percentage volume of nanoparticles on thermal conductivity and viscosity was examined in MD simulations of gaseous and supercritical Fe<sub>2</sub>O<sub>3</sub>-CO<sub>2</sub> nanofluids. The simulations were done using a temperature between 350-750 K. The experimental results are compared with the estimated thermophysical parameters of the base fluid for gas and supercritical CO<sub>2</sub> in fig. 2(a) [20]. In addition, this section discusses results obtained at 550 K to study the impact of percentage volume of nanoparticles. The thermal conductivity and viscosity of the Fe<sub>2</sub>O<sub>3</sub>-CO<sub>2</sub> nanofluid at 550 K are shown in fig. 2, with  $\phi$  ranging from 0.9% to 2.5%. Thermophysical properties of nanofluids are enhanced with increasing np  $\phi$  and np diameter, as illustrated in fig. 2. Amazingly, the range forecast by the molecular dynamics models agree with the predictions of the classical models (Maxwell and Hamilton and Crosser). The gaseous phase exhibits a stronger influence of  $\phi$  than the supercritical phase.

Figure 3 displays percentage volume of 1.526 and 2.72% at 550 K as a function of np diameter. Both the np diameter and  $\phi$  grow monotonically with the thermophysical characteristics of the Fe<sub>2</sub>O<sub>3</sub>-CO<sub>2</sub> nanofluid, as shown by the observations. Even though the np diameter stays the same, the current nanofluid exhibits bigger  $k$  and  $\mu$  at higher  $\phi$  than lower  $\phi$ . The thermophysical characteristics of the gaseous and supercritical Fe<sub>2</sub>O<sub>3</sub>-CO<sub>2</sub> nanofluid are shown to improve with increasing  $n_p$  diameter, as can be seen from the graphs.

Consistent with previous experimental literatures, the MD results demonstrate that the thermophysical characteristics of the present nanofluid improve as the np diameter increases [21]. A density distribution investigation close to the np was conducted to investigate the improvement's source. To determine the highest density ratio at the np, we considered several bin sizes in this scenario. The results demonstrate the formation of an ordered layer close to the solid surface, the thickness of which grows in relation the  $Z_p$  diameter. For bigger nanoparticles, the dense layer surrounding the nanoparticles is more organised, whereas for smaller ones, the density proportion is greater. One possible interpretation is that the created nanolayer enhances the effective  $\phi$ . The thickened nanolayer that results from an increase in np diameter is likely responsible for the observed improvement in thermophysical characteristics. One needs to know how thick the CO<sub>2</sub> layer is around the Fe<sub>2</sub>O<sub>3</sub> nanoparticles before they can see this impact. According to the range of np sizes (1.5-6.5 nm), the resulting layer thickness is between 0.4 nm



**Figure 3. The fluctuation of  $k$  and  $\mu$  of nanofluids with respect to nanoparticles diameter at various percentage volume at supercritical stage**



**Figure 4.** Nanolayer thickness and density ratio as a function of np diameter can vary

np diameter grows larger. The table displays the results of the relationship between the thickened nanolayer and diameter, as determined by eq. (15). In line with our previous results [22], this thicker layer is probably responsible for the enhanced thermophysical characteristics of the current nanofluid.

and 2 nm. The resultant VMD-formed nanolayer encircling the nanoparticles is shown in fig. 4. Equation (15) is utilised to assess the impact of nanolayer density on np size:

$$\rho_{nf} = \frac{N_{\text{molecules}} \cdot 44 \cdot 10^{-3}}{N_A V} \quad (15)$$

where  $N_A$  is the Avogadro number,  $N$  – the molecules number of  $\text{CO}_2$  molecules, and  $V$  – the spherical bin volume.

The density ratio,  $(\rho_n/\rho_f)$ , and the nanolayer thickness, as a function of the np diameter, are displayed in tabs. 3 and 4, respectively. According to the MD data, the density ratio drops and the nanolayer thickness rises as the

**Table 3.** Different diameters of the atom density of the nanolayer  $\text{Al}_2\text{O}_3\text{-CO}_2$

Diameter of nanoparticles	Nanolayer thickness [nm]	Density ratio, $(\rho_n/\rho_f)$
1.5	0.5	8.5
2.5	0.9	3.6
3.5	1.4	3.2
4.5	1.8	1.8
5.5	1.9	1.45
6.5	2.1	1.18

**Table 4.** Details of the utilised data

Factors	Temperature	$\phi$	np size	$k_{nf}$	$\mu_{nf}$
Mean	471	1.8	3.6	47.4	39.2
Count	240	240	240	240	240
Standard deviation	144	0.7	1.8	10.51	8.9
0%	300	0.8	1	31.7	25
25%	320	1.285	2	36.35	28
50%	475	1.66	4.5	49.39	41.9
75%	600	2.09	6	55.8	47
100%	700	2.7	7	66.9	53.8

A density ratio greater than 1 is achieved for each bin that is taken into account when determining the nanolayer thickness. (Since we have maintained a constant fluid density, the nanolayer thick with varying np are comparable for varying volume percentages).

**The machine learning of  $k$  and  $\mu$  of  $Fe_2O_3$  and  $CO_2$  carbon nanofluids**

*The information and modelling*

The MD simulations were performed to produce the data utilised for the models. Different input factors, including temperature,  $\phi$ , and np size, were used to generate 240 entries in total. The two factors of nanofluid,  $k$  and  $\mu$ , were found for these input attributes. A detailed report of the data was found that was utilised for exhibiting in tab. 4.

Pearson’s correlation was used to determine how well the variables were related to one another. Table 5 presents the values of the established correlations. According to the data in the table, the strongest positive association between the independent variable temperature and the nanoparticles’  $k$  and  $\mu$  is obvious. Three widely-used methods were employed for ML modelling: decision trees, K-nearest neighbours, and linear regression (LR). When it comes to supervised ML, the KNN is one of the most effective methods. It works well for both classification and regression tasks. Assuming that items that are comparable in proximity are close is the key to its operation [23]. Comparable to KNN in terms of classification and regression-based tasks, DT is an additional supervised learning technique. When making predictions about categorical outputs, DT like categorical variable decision trees can be useful. Continuous variable outputs were predicted using DT in this investigation. Predicting the dependent variable from a set of independent factors is the job of linear regression, the most basic type of supervised ML method. Single and multiple dependent variable predictions are both within its purview, *s.* Regression is referred to as multi-output regression when it predicts more than one output variable. Figure 5 displays the overall methodology of the models that were utilised.

**Table 5. Correlation between the variables**

	$n_p$ size	$\phi$	$k_{nf}$	Temperature	$\mu_{nf}$
$\phi$	$6.05 \cdot 10^{-18}$	1	0.115008	$-1.8 \cdot 10^{-17}$	0.150372
Temperature	0	$-1.8 \cdot 10^{-17}$	0.979746	1	0.964355
Nanoparticle size	1	$6.05 \cdot 10^{-19}$	0.123769	0	0.134057
$k_{nf}$	0.123769	0.115009	1	0.979746	0.992562
$\mu_{nf}$	0.133056	0.150372	0.992562	0.964355	1

Two data frames,  $X$  and  $y$ , were used to store the data after it was separated into independent (input) and dependent (output) parts (output). A subset of the data frames (using 15% of the total) was subsequently designated for testing, while the remaining 85% were earmarked for training. Out of a total of 240 entries, 204 were used for training the model and 36 were used for testing in the work. Before being fed into the models, the split data was standard-scaled and made up of two arrays: one for training and one for testing. The model was trained using the  $X$  train and  $y$  train arrays. These arrays stood for the independent and dependent variables, respectively, and contained 240 dataset iterations. To test the models, we used the  $X$  test array, which contained 36 dataset entries, as an independent variable and the  $y$  test array, which contained 36 dataset entries, as a dependent variable.

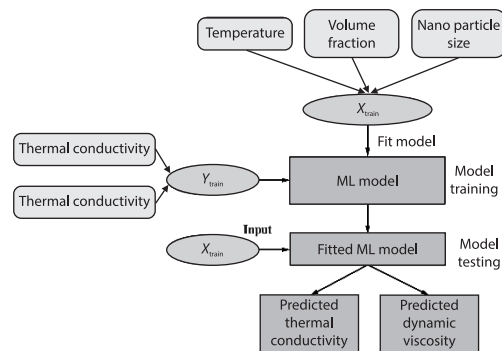


**Figure 5. Flowchart of the proposed models**

### Model outcomes and analysis

Few of the popular determination factors, including  $R^2$ , MSE, RMSE, and MAE, were used to examine the performance of the models that were built (MAE). Table 6 displays the determination coefficients. While all of the models have done adequately, the table shows that the DT model outperforms them all. It has an  $R^2$  value of 0.99 and can predict both  $k$  and  $\mu$ . Onp of that, graphs are created to show how well the models forecast, figs. 6(a)-6(f).

**Table 6. Coefficients for determining developed models**

Model	KNN	LR	DT
$R^2$	0.99662	0.98168	0.98099
RMSE	1.07427	1.55822	0.8834
MSE	1.14267	2.38698	0.77282
MAE	0.88421	1.21574	0.78667

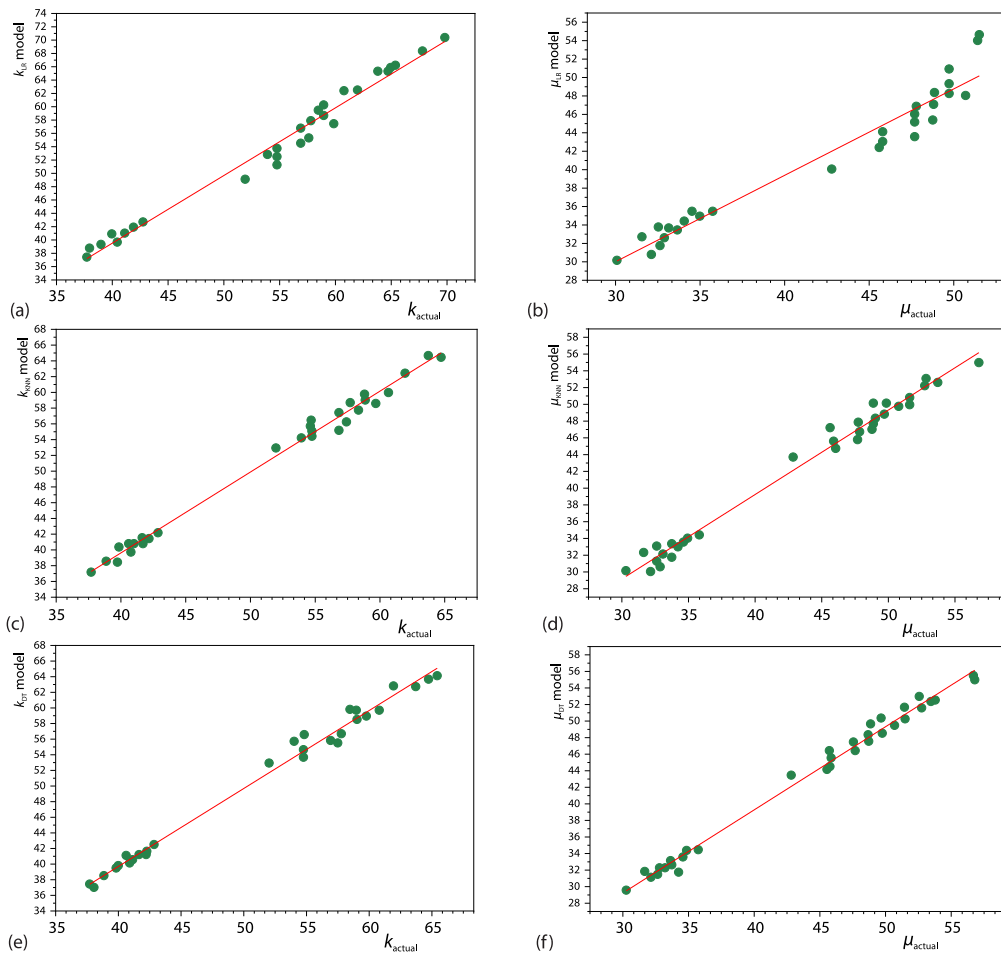


**Figure 6. The observed values of  $k$  and  $\mu$  as predicted by the (a) and (b) DT model, (c) and (d) KNN model, and (e) and (f) LR model**

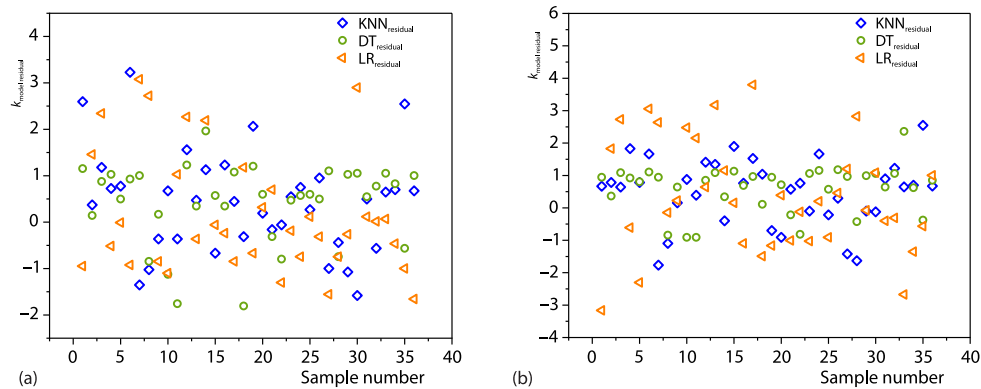


Figure 7. Residual plots for (a) thermal conductivity model and (b) viscosity model

Figures 6(a) and 6(b) demonstrate that the DT model outperforms KNN in predicting both parameters,  $k$  and  $\mu$ , with an accuracy of 0.99. The suitability of the KNN model for forecasting both  $k$  and  $\mu$  is illustrated in fig. 6(c) and 6(d). The model achieves a comparable efficiency of 0.98 in making these predictions. The LR model predicts the  $k$  with a maximum degree of accurateness than the  $\mu$ , as can be indicates in figs 6(e) and 6(f). The accuracy for  $\mu$  is 0.956, whereas the model predicts  $k$  with a precision of 0.9841. With all of the LR models working together, the prediction efficiency is 0.971.

Figure 7 show the residual graph for  $k$  and  $\mu$ , respectively, to illustrate the variation in prediction among the various models. Model DT clearly has the lowest overall variance out of the three.

## Conclusion

This research makes use of molecular dynamics simulations in the Green-Kubo formalism to examine the thermophysical parameters ( $k$  and  $m$ ) of an  $\text{Fe}_2\text{O}_3\text{-CO}_2$  nanofluid. For the gaseous phases, the temperature was adjusted between 300 K and 330 K, while for the supercritical phase, it was altered between 450 K and 700 K, with varying pressures. The effect on the nanofluid's  $k$  and  $\mu$  of variables like temperature,  $u$ , and np size is investigated. In order to compare the findings from MD simulations with those from the present study, the researchers also used a ML approach. To summarise, the main results of this study are: by analysing the density of the gas, there is a thick layer of  $\text{CO}_2$  molecules close to the np was found. For particle diameter systems of 1.5 nm, 2.5 nm, 3.5 nm, 4.5 nm, 5.5 nm, and 6.5 nm dimensions, the resulting nanolayer thickness is 0.5 nm, 0.9 nm, 1.4 nm, 1.7 nm, 1.9 nm, and 2 nm, in that order. An increase in temperature,  $\varphi$ , and np size resulted to an improvement in the  $k$  and  $\mu$  of the  $\text{Fe}_2\text{O}_3\text{-CO}_2$  nanofluid. When comparing the gaseous and supercritical phases, the improvement is smaller in the latter. The LR model's dismal overall accuracy of 0.97 and its inconsistent effectiveness in predicting  $k$  and  $\mu$  make it unfit to be included in the list of created models. To forecast the parameters, KNN, DT and two more models were used, since they are just as good in  $k$  and  $\mu$  forecasting. When predicting the  $k$  and  $\mu$  of  $\text{Fe}_2\text{O}_3\text{-CO}_2$  nanofluids at volume fractions, and nanoparticle sizes and various temperatures, the top-performing Decision tree model can save a lot of time and effort compared to the lengthy simulation approach. Enhancements to the thermophysical properties of  $\text{Fe}_2\text{O}_3\text{-CO}_2$  Nanofluid could result in an improvement in oil recovery and make it a more effective refrigerant compared to conventional  $\text{CO}_2$ .

## References

- [1] Zhang, Y., Xu, X., Machine Learning Specific Heat Capacities of Nanofluids Containing CuO and Al<sub>2</sub>O<sub>3</sub>, *AIChE Journal*, 67 (2021), 9
- [2] Mukesh, P. C., et al., Prediction of Nanofluid Viscosity Using Multilayer Perceptron and Gaussian Process Regression, *Journal Therm. Anal. Calorim.*, 144 (2021), 4, pp. 1151-1160
- [3] Kanti, P., et al., Thermal Performance of Hybrid Fly Ash and Copper Nanofluid in Various Mixture Ratios: Experimental Investigation And Application of a Modern Ensemble Machine Learning Approach, *International Communications in Heat and Mass Transfer*, 129 (2021), 105731
- [4] Wadi, V. T., et al., Experimental Study and Computational Intelligence on Dynamic Viscosity and Thermal Conductivity of Hnts Based Nanolubricant, *Industrial Lubrication and Tribology*, 74 (2022), 1, pp. 102-110, 100501
- [5] Kanti, P. K., et al., Thermophysical Profile of Graphene Oxide and MXene Hybrid Nanofluids for Sustainable Energy Applications: Model Prediction with a Bayesian Optimized Neural Network with K-Cross fold Validation, *FlatChem*, 39 (2023), 100501
- [6] Mukesh Kumar, P. C., Kavitha, R., Regression Analysis for Thermal Properties of Al<sub>2</sub>O<sub>3</sub>/H<sub>2</sub>O Nanofluid Using Machine Learning Techniques, *Heliyon*, 6 (2020), 6
- [7] Adun, H., et al., An Experimental Investigation of Thermal Conductivity and Dynamic Viscosity of Al<sub>2</sub>O<sub>3</sub>-ZnO-Fe<sub>3</sub>O<sub>4</sub> Ternary Hybrid Nanofluid and Development of Machine Learning Model, *Powder Technol.*, 394 (2021), Dec., pp. 1121-1140
- [8] Wang, X., et al., A Comprehensive Review on the Application of Nanofluid in Heat Pipe Based on the Machine Learning: Theory, Application and Prediction, *Renewable and Sustainable Energy Reviews*, 150 (2021), 111434
- [9] Said, Z., et al., Recent Advances in Machine Learning Research for Nanofluid Heat Transfer in Renewable Energy, in: *Advances in Nanofluid Heat Transfer*, Elsevier, Amsterdam, The Netherlands, 2022, Chapter 7, pp. 203-228
- [10] Zhang, Z., et al., Optimized ANFIS Models Based on Grid Partitioning, Subtractive Clustering, And Fuzzy C-Means to Precise Prediction of Thermophysical Properties of Hybrid Nanofluids, *Chemical Engineering Journal*, 471 (2023), 144362
- [11] Said, Z., et al., Experimental Analysis of Novel Ionic Liquid-MXene Hybrid Nanofluid's Energy Storage Properties: Model-Prediction Using Modern Ensemble Machine Learning Methods, *Journal Energy Storage*, 52 (2022), 104858
- [12] Sahin, F., et al., From Experimental Data to Predictions: Artificial intelligence Supported New Mathematical Approaches for Estimating Thermal Conductivity, Viscosity and Zeta Potential in Fe<sub>3</sub>O<sub>4</sub>-Water Magnetic Nanofluids, *Powder Technol.*, 430 (2023), 118974
- [13] Adun, H., et al., Estimation of Thermophysical Property of Hybrid Nanofluids for Solar Thermal Applications: Implementation of Novel Optimizable Gaussian Process Regression (O-GPR) Approach for Viscosity Prediction, *Neural Comput. Appl.*, 34 (2022), 13, pp. 11233-11254
- [14] Jamei, M., Said, Z., Recent Advances in the Prediction of Thermophysical Properties of Nanofluids Using Artificial Intelligence, in: *Hybrid Nanofluids: Preparation, Characterization and Applications*, Elsevier, Amsterdam, The Netherlands, 2022, Chapter 9, pp. 203-232
- [15] Shi, L., et al., Thermo-Physical Properties Prediction of Carbon-Based Magnetic Nanofluids Based on an Artificial Neural Network, *Renewable and Sustainable Energy Reviews*, 149 (2021), 111341
- [16] Li, J., et al., Prediction and Optimization of the Thermal Properties of TiO<sub>2</sub>/Water Nanofluids in the Framework of a Machine Learning Approach, *Fluid Dynamics and Materials Processing*, 19 (2023), 8, Chapter 9, pp. 2181-2200
- [17] Bhanuteja, S., et al., Prediction of Thermophysical Properties of Hybrid Nanofluids Using Machine Learning Algorithms, *International Journal on Interactive Design and Manufacturing*, On-line first, <https://doi.org/10.1007/312008-023-01293-w>, 2023
- [18] Onyiriuka, E., Modelling the Thermal Conductivity of Nanofluids Using a Novel Model of Models Approach, *Journal Therm. Anal. Calorim.*, 148 (2023), Nov., pp. 13569-13585
- [19] Colak, A. B., et al., Prediction of Nanofluid-Flows' Optimum Velocity in Finned Tube-in-Tube Heat Exchangers Using Artificial Neural Network, *Kerntechnik*, 88 (2023), 1, pp. 100-113
- [20] Girimurugan, R., et al., Application of Deep Learning to the Prediction of Solar Irradiance through Missing Data, *International Journal of Photoenergy*, 2023 (2023), 4717110
- [21] Alghamdi, W., et al., Turbulence Modelling through Deep Learning: An in-Depth Study of Wasserstein GAN, *Proceedings*, 4<sup>th</sup> Int. Conf. on Smart Electronics and Communication, Trichy, India, 2023, pp. 793-797

- [22] Malek, N. A., *et al.*, Low-Dimensional Nanomaterials For Nanofluids: A Review of Heat Transfer Enhancement, *Journal Therm. Anal. Calorim.*, 148 (2023), 19, pp. 9785-9811
- [23] Ganga, S., *et al.*, Modelling of Viscosity and Thermal Conductivity of Water-Based Nanofluids Using Machine-Learning Techniques, *International Journal of Mathematical, Engineering and Management Sciences*, 8 (2023), 5, pp. 817-840